Renewable Energy 101 (2017) 1013–1020

Contents lists available at ScienceDirect

Renewable Energy

journal homepage: www.elsevier.com/locate/renene

Scaling of slow-drift motion with platform size and its importance for floating wind turbines

R.C. Lupton*, R.S. Langley

Department of Engineering, University of Cambridge, Trumpington St, Cambridge, CB2 1PZ, UK

ARTICLE INFO

Article history:
Received 25 March 2016
Received in revised form
14 September 2016
Accepted 23 September 2016

Keywords:
Floating wind turbines
Offshore wind
Wind energy
Slow drift
Frequency-domain modelling
Second-order hydrodynamics

ABSTRACT

Slow drift is a large, low-frequency motion of a floating platform caused by nonlinear hydrodynamic forces. Although slow drift is a well-known phenomenon for ships and other floating structures, new platforms for floating wind turbines are significantly smaller in scale, and it is yet to be established how important slow drift is for them. In this paper we derive an approximate expression for the scaling of the slow drift motion with platform size, mooring characteristics and wave conditions. This suggests that slow drift may be less important for floating wind turbines than other, larger, floating structures. The accuracy of the approximations is discussed; in the one case where detailed data is available, the approximate result is found to be conservative by a factor of up to 40.

1. Introduction

Floating wind turbines are increasingly of interest for their ability to access wind resources over deep water. Their development draws on both existing fixed-base wind turbines and other types of floating platforms, but introduces additional modelling challenges which require the development of new modelling tools. In this paper we consider the importance of the 'slow drift motion' for floating wind turbines; a wider discussion of modelling floating wind turbines is given in Ref. [1].

Slow drift is a large, low-frequency motion of a floating platform caused by nonlinear hydrodynamic forces which excite a resonant motion of the moored platform [2, chapter 5]. These second-order forces are much smaller than the main hydrodynamic loading, but occur at low frequencies where there is otherwise little excitation. Since there is typically little damping in the low-frequency modes of the moored platform, the response can be large despite the small magnitude of the forces. Slow drift is therefore one of the three main components of the loadings and motion in a mooring system, alongside static and wave-frequency forces [3]. Although we focus here on the low-frequency forces, there are similar high-frequency nonlinear forces which can excite structural vibration models of the structure [2].

As well as its practical importance for design, this motion presents challenges in modelling. In the time domain, the low frequency of the motion means that very long simulations are needed to properly capture the behaviour. In the frequency domain, although the spectrum of the nonlinear forces can be calculated fairly easily, the statistics are non-Gaussian, which adds a little to the difficulty of predicting the response. It is therefore useful to know how significant the slow drift motion can be for floating wind turbines. Note that it is not necessary to neglect it completely to achieve simplifications: in the frequency domain, simplifications can be made if the slow drift motion is small compared to the wave frequency motion, and its statistics can be approximated as Gaussian.

Although slow drift is well-known in traditional floating offshore structures, it has been studied in only a few cases for floating wind turbines. Lucas [4] calculated the first- and second-order response of the OC3-Hywind spar-buoy [5] and a semisub platform, using the commercial panel code WAMIT [6] together with an in-house code, for three regular-wave and three irregular-wave conditions. More recently, motivated by observations of possible second-order effects in scale model tests [7], Roald et al. [8] calculated first- and second-order forces and responses for two specific floating wind turbine designs, the same OC3-Hywind spar

* Corresponding author.
E-mail address: rcl33@cam.ac.uk (R.C. Lupton).

http://dx.doi.org/10.1016/j.renene.2016.09.052

buoy, and a tension-leg platform (TLP). They also used WAMIT, together with linearised system matrices calculated by the wind turbine code FAST [9]. Although FAST does not yet account for second-order hydrodynamics, this is being addressed [10]. Bayati et al. [11] apply the same approach to a semisub platform.

The conclusions of these results for the different platforms and wave conditions vary: in some cases the slow drift response is smaller than the first-order motion, and in some cases it is larger. This contrasts with the expectation for traditional floating structures that the slow drift motion is large compared to the first-order motion, albeit for only the few results which are available. We suggest this difference in behaviour may be due to the significant difference in scale between floating wind turbines and other floating structures: some can be an order of magnitude larger than floating wind turbine platforms, while ships can be even larger.

To our knowledge there is no particular discussion in the literature of how slow drift motion scales with the size of the floating platform. In this paper, we derive an expression which approximates the scaling of the slow drift motion with platform size, mooring characteristics and wave conditions. While the studies mentioned above give results for particular platform designs and wave conditions, we aim to give a more general result. To do this several approximations and assumptions have been made, so the result is only an approximation. We conclude by discussing the expected accuracy of these approximations.

Frequency-domain models of floating wind turbines, whether or not they include second-order hydrodynamics, have previously limited themselves to the rigid-body dynamics of the floating platform [1]. Although this is often reasonable, it has sometimes been presented as a limitation of the frequency-domain approach itself. We therefore note that the approach described here is capable of including the flexibility of the structure, and give an example of the 'OC3-Hywind' floating wind turbine mentioned above.

Before beginning we should put these second-order low-frequency forces into perspective on a wind turbine. As Roald et al. [8] show, when the turbine is operating the low-frequency aerodynamic forces on the rotor are much larger than the low-frequency hydrodynamic forces, making the second-order hydrodynamic forces unimportant. However, they are still of interest whenever the turbine is not operating. This may be due to high wind speeds (in extreme environmental conditions), or due to faults (under any environmental conditions).

2. Frequency-domain model of flexible structure

The basic form of the frequency domain model is

$$\left\{ -\omega^2 \boldsymbol{M} + i\omega \boldsymbol{B} + \boldsymbol{K} \right\} \overline{\boldsymbol{q}}(\omega) = \overline{\boldsymbol{F}}(\omega) \tag{1}$$

or equivalently

$$\overline{\boldsymbol{q}}(\omega) = \boldsymbol{H}(\omega) \overline{\boldsymbol{F}}(\omega) \tag{2}$$

where $\boldsymbol{H}$ is the system transfer function matrix, and $\overline{\boldsymbol{q}}$ and $\overline{\boldsymbol{F}}$ are the complex amplitude of the response and applied force for sinusoidal motion at frequency ω:

$$\boldsymbol{F} = \overline{\boldsymbol{F}}(\omega) e^{i\omega t} \tag{3a}$$

$$\boldsymbol{q} = \overline{\boldsymbol{q}}(\omega) e^{i\omega t} \tag{3b}$$

with the convention that the real part is assumed. If the cross-spectral density of the force is $\boldsymbol{S}_{\boldsymbol{FF}}(\omega)$, the cross-spectral density of the system response can be found as [12, chapter 6]:

$$\boldsymbol{S}_{\boldsymbol{qq}}(\omega) = \boldsymbol{H}(\omega) \boldsymbol{S}_{\boldsymbol{FF}}(\omega) \boldsymbol{H}^{*T}(\omega) \tag{4}$$

where ^{*T} indicates the complex conjugate transpose. The response variances can then be found from the covariance matrix,

$$\mathrm{E}\left[\boldsymbol{q}\boldsymbol{q}^T\right] = \mathrm{Re} \int_0^\infty \boldsymbol{S}_{\boldsymbol{qq}}(\omega) \mathrm{d}\omega \tag{5}$$

These equations are very general. Next, the parts of the equation of motion (1) will be defined in more detail in relation to a general floating structure. Then the frequency-domain model is applied to an example floating wind turbine.

2.1. Equations of motion of a floating structure

For a flexible structure with hydrodynamic loading, the mass, damping and stiffness matrices which appear in Equation (1) can be written as

$$\boldsymbol{M} = \boldsymbol{M}_{\mathrm{struct}} + \boldsymbol{A}_{\mathrm{h}}(\omega) \tag{6a}$$

$$\boldsymbol{B} = \boldsymbol{B}_{\mathrm{struct}} + \boldsymbol{B}_{\mathrm{h}}(\omega) + \boldsymbol{B}_{\mathrm{v}} \tag{6b}$$

$$\boldsymbol{K} = \boldsymbol{K}_{\mathrm{struct}} + \boldsymbol{K}_{\mathrm{h}} + \boldsymbol{K}_{\mathrm{m}} \tag{6c}$$

Here $\boldsymbol{A}_{\mathrm{h}}$ and $\boldsymbol{B}_{\mathrm{h}}$ are the hydrodynamic added mass and radiation damping matrices; $\boldsymbol{B}_{\mathrm{v}}$ is a linearised viscous damping matrix; $\boldsymbol{K}_{\mathrm{h}}$ is the hydrostatic stiffness matrix; $\boldsymbol{K}_{\mathrm{m}}$ is the linearised mooring line stiffness; and $\boldsymbol{M}_{\mathrm{struct}}$, $\boldsymbol{B}_{\mathrm{struct}}$ and $\boldsymbol{K}_{\mathrm{struct}}$ are the structural mass, stiffness and damping matrices. Most commonly the submerged part of the structure will be assumed rigid and the hydrodynamic, hydrostatic and mooring matrices will contain only the terms relating to the six rigid-body degrees of freedom, while the structural system matrices will in general relate to all the degrees of freedom of the structure.

The applied forces consist of aerodynamic loads on the wind turbine rotor, wave excitation forces, and viscous drag forces. Here we ignore aerodynamic and viscous forces, although they could be included given a suitable linearisation. Mooring line forces are assumed to be accounted for by the linearised stiffness matrix $\boldsymbol{K}_{\mathrm{m}}$ and are not counted as applied forces here. Correct to second order, the wave excitation forces can be written as the first two terms in a Volterra series,

$$\boldsymbol{F}(t) = \int_{-\infty}^{\infty} \boldsymbol{H}_1(\omega) \zeta(\omega) e^{i\omega t} \mathrm{d}\omega + \int_{-\infty}^{\infty} \int_{-\infty}^{\infty} \boldsymbol{H}_2(\omega_1, \omega_2) \zeta(\omega_1) \zeta(\omega_2) e^{i(\omega_1+\omega_2)t} \mathrm{d}\omega_1 \mathrm{d}\omega_2 \tag{7}$$

where $\zeta(\omega)$ is the Fourier transform of the sea surface elevation, and $\boldsymbol{H}_1(\omega)$ and $\boldsymbol{H}_2(\omega_1,\omega_2)$ are the Fourier transforms of the first- and second-order Volterra kernels [13]. This shows that the wave loading consists of forces at ω which are linear in the wave amplitudes, and forces at $\omega_1 + \omega_2$ which are second order in the wave amplitudes. Because the range of the integrals above is from $-\infty$ to ∞, the second-order forces occur at both the sum and difference frequencies of the waves. The difference-frequency forces are of particular interest because they can excite large platform motions. Although in future it may be of interest to include sum-frequency forces, they are not considered further at present.

The wave forces are more commonly written in terms of the wave excitation coefficients $\boldsymbol{X}(\omega)$ and the quadratic transfer functions (QTFs) $\boldsymbol{T}(\omega_1,\omega_2)$, which are directly related to the formal Volterra kernels $\boldsymbol{H}_1$ and $\boldsymbol{H}_2$ [14]:

$$\boldsymbol{H}_1(\omega) = \boldsymbol{X}(\omega) \tag{8a}$$

$$\boldsymbol{H}_2(\omega_1, -\omega_2) = 2\boldsymbol{T}(\omega_1, \omega_2) \tag{8b}$$

The spectrum of the first-order forces is

$$\boldsymbol{S}_{\boldsymbol{FF}}^{(1)}(\omega) = \boldsymbol{X}(\omega) S_{\zeta\zeta}(\omega) \boldsymbol{X}(\omega)^{*T} \tag{9}$$

Pinkster [15] shows that the second-order force spectrum is

$$\boldsymbol{S}_{\boldsymbol{FF}}^{(2)}(\omega) = 8 \int_0^\infty \boldsymbol{T}(\omega', \omega' + \omega) S_{\zeta\zeta}(\omega') S_{\zeta\zeta}(\omega' + \omega)\, \boldsymbol{T}(\omega', \omega' + \omega)^{*T} \mathrm{d}\omega' \tag{10}$$

where $S_{\zeta\zeta}(\omega)$ is the wave power spectrum.

Calculation of the full QTF matrix $\boldsymbol{T}(\omega_1,\omega_2)$ can be time consuming, so sometimes an approximation known as Newman's approximation is used [2, chapter 5]:

$$\boldsymbol{T}(\omega_1, \omega_2) \approx \boldsymbol{T}(\omega_2, \omega_1) \approx \frac{\boldsymbol{T}(\omega_1, \omega_1) + \boldsymbol{T}(\omega_2, \omega_2)}{2} \tag{11}$$

This can give satisfactory results because in most cases it is the low frequency forces that are of interest, for which ω_1 is close to ω_2.

Although in general the first and second order forces vary with the angle of approach of the waves, we consider here only unidirectional waves.

2.2. First and second order motion of a floating wind turbine

The equations above apply to any floating structure. We now consider the application to a floating wind turbine; as a specific example the OC3-Hywind reference turbine defined by the OC3 project is used [5]. The first- and second-order response is found, and verified by comparison to published results for this turbine. In this case the second-order motion will be shown to be small compared to the first-order motion, which would be, as discussed in the introduction, an unusual result for floating oil & gas platforms.

The structural matrices are found by building a multibody structural model [1]. The layout of the model is shown in Fig. 1. All parameters are supplied by the OC3 project [5]. From this multibody model the matrices $\boldsymbol{M}_{\text{struct}}$, $\boldsymbol{B}_{\text{struct}}$ and $\boldsymbol{K}_{\text{struct}}$ are found by numerical linearisation.

The hydrodynamic coefficients are typically calculated by a numerical panel method code. The details are not presented here, since data is published by the OC3 project for $\boldsymbol{A}_{\text{h}}(\omega)$, $\boldsymbol{B}_{\text{h}}(\omega)$, $\boldsymbol{K}_{\text{h}}$ and $\boldsymbol{X}(\omega)$, as well as the linearised mooring line stiffness $\boldsymbol{K}_{\text{m}}$. The diagonals of the QTFs are provided by Lucas [4]; the full matrix $\boldsymbol{T}(\omega_1,\omega_2)$ is reconstructed using Newman's approximation (Equation (11)).

Fig. 2 shows an example of the first- and second-order hydrodynamic forces on the platform. They have been calculated for a JONSWAP wave spectrum with a significant wave height of 4 m and a peak period of 6 s. The waves are unidirectional and aligned with the surge axis; because the platform is symmetric, the sway and roll forces are zero.

Some of the platform transfer functions are plotted in the top of Fig. 3. Peaks at the surge, pitch and heave natural frequencies are visible. The frequencies match well with published results from the OC3 code-comparison project, shown by Table 2 and Fig. 4.

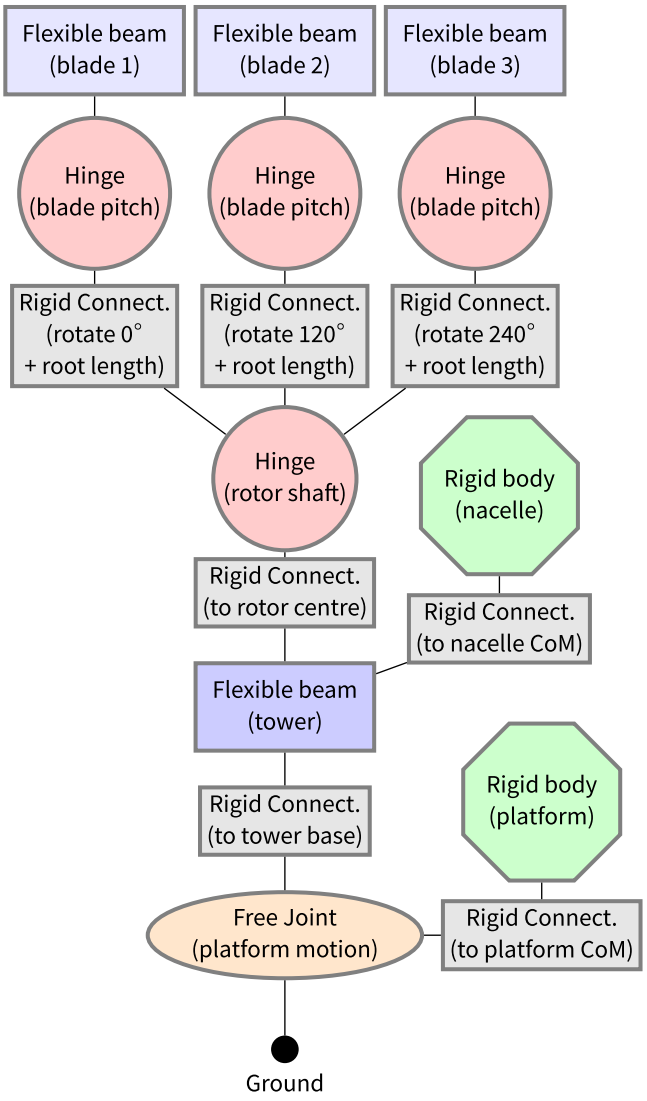

Fig. 1. Elements making up the multibody model of the flexible floating wind turbine. The free joint defines the position and orientation of the platform origin, located at the mean water level. The bottom of the flexible part of the tower, and the centre of mass of the platform, are offset from this origin by rigid connections. The 'nacelle' contains the gearbox, bearings and generator at the tower top. 'Root length' refers to the radial distance from the rotor axis to the start of the flexible blade.

Also shown in Fig. 3 are the response power spectra for platform motion in surge, heave and pitch, as well as the tower-top elastic deflection. Results provided by OC3 from simulations in FAST are shown by the black lines. Generally there is a good match, although the frequency resolution in the FAST results is low, and the dynamic range of the plots is large.

The slow drift motion is visible as the peaks at the left, corresponding to the platform natural frequencies in surge and pitch. Although in general the low-frequency motion can be large compared to the wave-frequency response [3, chapter 9], here the low-frequency peaks in Fig. 3 and rms values in Table 1 are relatively small. This is the motivation for the following section which aims to understand if this is due to the smaller scale of floating wind turbines.

3. Scaling of slow drift motions

We now return to investigate the scaling of slow drift motions with platform size, mooring characteristics and wave conditions.

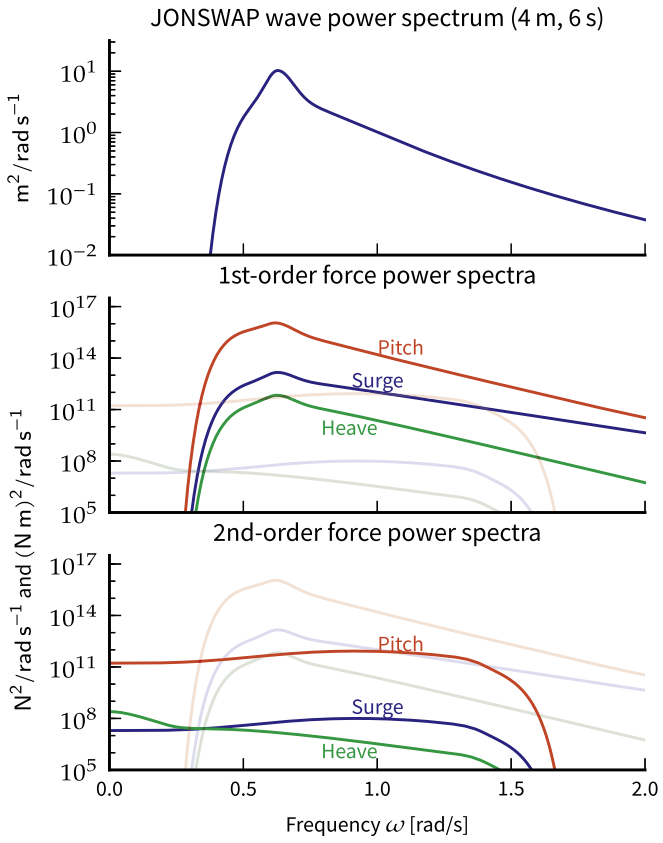

Fig. 2. Example of OC3-Hywind platform forces for one wave spectrum. The second-order forces are about 10^5 times smaller than the first-order forces in the wave frequency range, but at low frequencies they are the only source of wave loading.

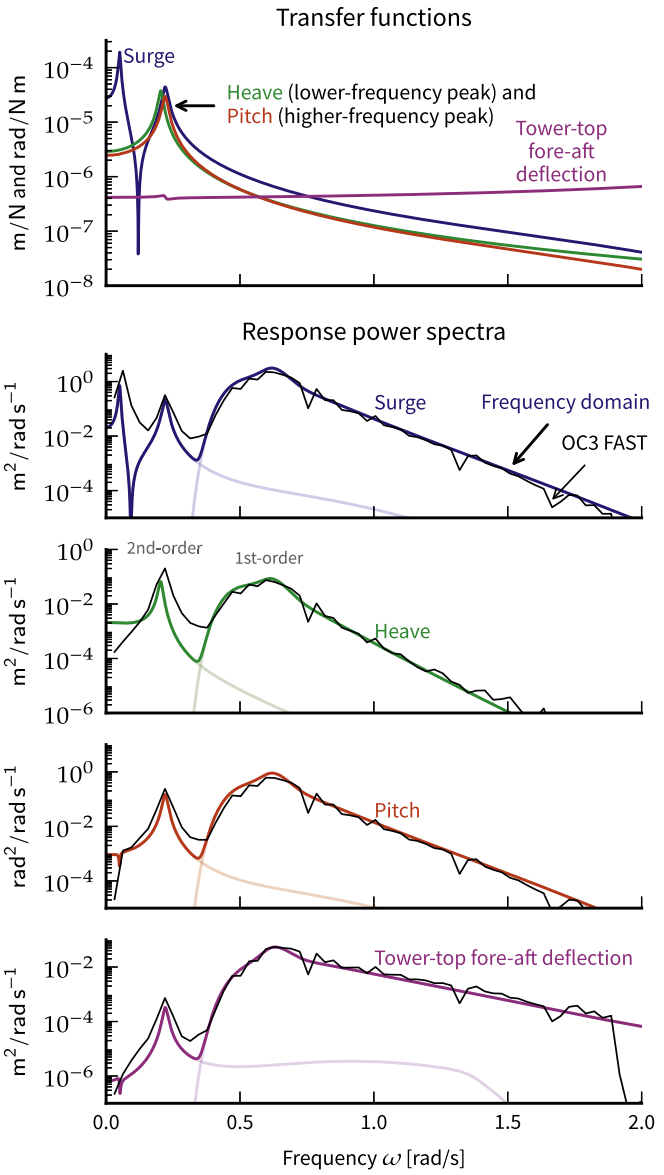

Fig. 3. OC3-Hywind platform transfer functions, and responses corresponding to forces shown in Fig. 2. The response is the sum of the first- and second-order responses, which are also shown individually by faint lines. Published results from FAST simulations are shown by thin black lines.

Since the aim is to derive simple, approximate results, only motion in the surge direction is considered, and only platforms which are vertical cylinders of various draft and radius are considered. The natural frequency in surge is assumed to be low, and constant as the mass of the platform varies, since it is usually chosen to avoid the main wave forcing frequencies, which are independent of the size of the platform. Damping is also assumed to be small and independent of platform size.

Approximations for the mean surge force acting on the cylinder, and for the wave spectrum are also introduced below. The implications of these assumptions will be discussed further in Section 3.2 below.

3.1. Derivation of approximate response

Since for simplicity only the surge degree of freedom of the platform is considered, only the surge component of the second order force is required. The surge component of the spectrum $\boldsymbol{S}_{\boldsymbol{FF}}^{(2)}(\omega)$ is written $S^{(2)}(\omega)$. Aranha and Fernades [16] show that for small ω the spectrum is nearly flat,

$$S^{(2)}(\omega) = S_0 + O\left(\omega^2\right) \tag{12}$$

In general the slow drift response would be found from Equations (4) and (5), but because the surge motion is assumed to be lightly damped and the surge natural frequency is small, the slow drift response can be found using the white-noise approximation [12]:

Table 1
RMS first- and second-order response (m), as shown in Fig. 3.

Response	First order	Second order
Surge motion	0.546	0.013
Heave motion	0.015	0.002
Pitch motion	0.156	0.004
Tower-top fore-aft deflection	0.012	1.205×10^{-5}

$$\sigma_x^2 = \frac{\pi S_{\text{white}}}{4\zeta\omega_n^3 M^2} \tag{13}$$

where σ_x is the surge response standard deviation, S_{white} is the white-noise approximation of the surge force, M is the platform mass, and ζ and ω_n are the damping and natural frequency in surge respectively. The damping factor can include linearised viscous

Table 2
The first 16 OC3-Hywind platform natural frequencies. 'Bladed' and 'FAST' from OC3 published results, 'Current' are the results from the present model.

Mode (frequencies in rad/s)	Bladed	FAST	Current
Platform sway	0.075	0.051	0.051
Platform surge	0.050	0.051	0.051
Platform heave	0.207	0.204	0.204
Platform roll	0.199	0.215	0.221
Platform pitch	0.199	0.215	0.221
Platform yaw	0.767	0.760	0.763
1st tower side-to-side	2.827	2.874	3.131
1st tower fore-aft	2.890	2.973	3.112
1st blade asym. flapwise pitch	4.210	4.262	4.260
1st blade asym. flapwise yaw	3.990	4.364	4.467
1st blade collective flapwise	4.430	4.461	4.560
1st blade asym. edgewise pitch	6.943	6.793	6.991
1st blade asym. edgewise yaw		6.870	6.817
2nd blade asym. flapwise pitch	11.624	12.144	12.004
2nd blade asym. flapwise yaw		12.296	12.541
2nd blade collective flapwise	12.127	12.712	12.615

'Asymmetric flapwise pitch' is a mode where the blades move out of the rotor plane with a horizontal axis of symmetry; 'asymmetric flapwise yaw' is similar but with a vertical axis of symmetry. In the 'collective flap' modes all blades move out of the rotor plane together. The edgewise modes are analogous but with motion in the rotor plane.

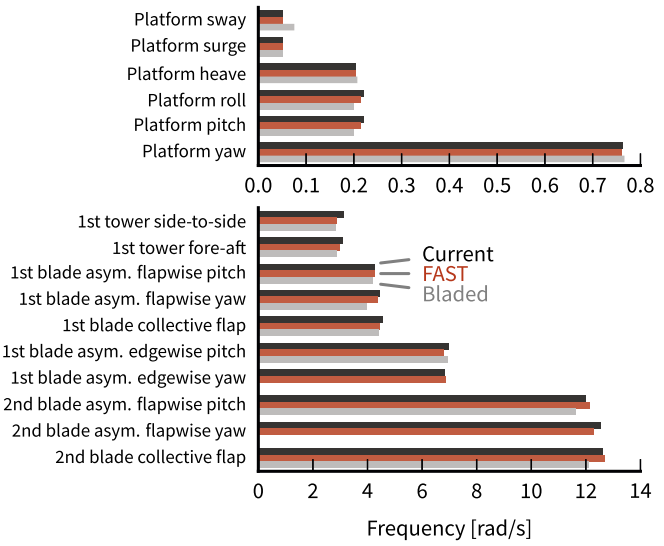

Fig. 4. The first 16 OC3-Hywind platform natural frequencies. See Table 2 for explanation.

damping effects, as well as other sources of damping. The use of the white-noise approximation is acceptable because the lightly-damped response is mostly determined by the forcing at the resonant frequency. Since the force spectrum is nearly flat (Equation (12)) and the resonant frequency is assumed small, the spectrum at zero frequency can be used: $S_{\text{white}} \approx S_0$.

The mass of the cylinder is assumed to be equal to its displacement:

$$M = \rho d \pi a^2 \tag{14}$$

where ρ is the density of water, d is the draft of the cylinder and a is the radius. Added mass, which depends non-trivially on the shape of the platform, increases the effective mass of the platform. However, since the focus of the analysis is on the effect of scale, rather than shape, added mass is neglected here.

The value of the second-order force spectrum at zero frequency is needed in Equation (13). It can be found from Equation (10) as

$$S_0 = S^{(2)}(0) = 8 \int_0^\infty S_{\zeta\zeta}^2(\omega') |T_{11}(\omega', \omega')|^2 \mathrm{d}\omega' = 8(\rho g a)^2 I \tag{15}$$

where

$$I = \int_0^\infty S_{\zeta\zeta}^2(\omega) D^2(\omega) \mathrm{d}\omega \tag{16}$$

in which $D(\omega)$ is the normalised mean surge force such that $T_{11}(\omega,\omega) = \rho g a D(\omega)$. We now introduce approximations for $D(\omega)$ and $S_{\zeta\zeta}(\omega)$ which allow this integral to be evaluated analytically.

The ISSC description of the wave spectrum is taken as a starting point [2, chapter 2]:

$$\frac{S_{\zeta\zeta}(\omega)}{H_s^2 T_m} = \frac{A}{2\pi} \left(\frac{\omega T_m}{2\pi}\right)^{-5} \exp\left(- b^4 \left(\frac{\omega T_m}{2\pi}\right)^{-4} \right) \tag{17}$$

where $A = 0.11$, $b^4 = 0.44$, H_s is the significant wave height and T_m is the mean wave period, defined in terms of the spectral moments $m_k = \int_0^\infty \omega^k S(\omega) \mathrm{d}\omega$ as $T_m = 2\pi m_0 / m_1$ and $H_s = 4\sqrt{m_0}$. This description of the wave spectrum allows the two parameters T_m and H_s to be specified independently. Sometimes a one-parameter wave spectrum is used, in which case the following relationship can be used [[17], chapter 3; 2, chapter 2]:

$$T_m = 3.84 \sqrt{H_s} \tag{18}$$

The exact shape of the wave spectrum is not a concern here; rather the aim is to find an approximate but closed-form result. Therefore for analytical convenience the wave spectrum is approximated by a uniform rectangular spectrum of height C between ω_1 and ω_2 (Fig. 5, left), which matches the first three spectral moments. It can be shown that

$$\omega_1 = (1 - Kb)\omega_m \tag{19a}$$

$$\omega_2 = (1 + Kb)\omega_m \tag{19b}$$

$$C = \frac{A H_s^2}{8 b K \omega_m} \tag{19c}$$

where $K^2 = 3\sqrt{\pi} - 3\Gamma^2(3/4)$ and the mean wave frequency is $\omega_m = 2\pi / T_m$. $\Gamma(x)$ is the gamma function.

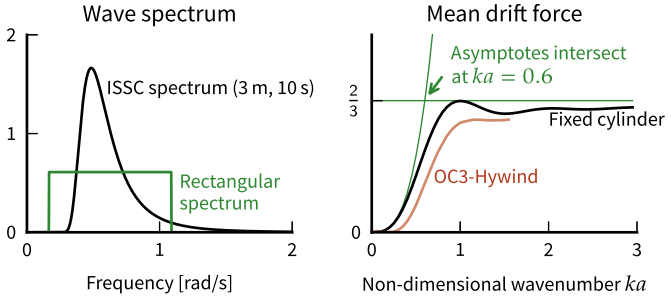

Fig. 5. Approximations introduced in deriving the slow drift motion results. On the left, the wave spectrum is approximated by a rectangular spectrum which matches the first three spectral moments. On the right, the mean drift force is approximated by the two asymptotes. OC3-Hywind data from Ref. [4].

For simplicity the mean surge force on a fixed bottom-piercing cylinder is used as an estimate of $D(\omega)$, although it is recognised that this is only an approximation of the more complex force on the moving platform. The mean force can then be written as a sum of Bessel and Hankel functions [18], but is not in a form which is easily integrable. Instead it is approximated by the two asymptotes shown in the right of Fig. 5:

$$D(ka) \approx \begin{cases} \dfrac{2}{3} & \text{for large } ka \\ \dfrac{5\pi^2}{16}(ka)^3 & \text{for small } ka \end{cases} \tag{20}$$

where ka is the non-dimensional frequency, which in deep water is related to angular frequency ω by $ka = \omega^2 a/g$ [2,19]. The two asymptotes meet when $ka = 0.6$, which corresponds to a frequency of $\omega_X = (0.6g/a)^{1/2}$. Note that these asymptotes are conservative for all values of ka, although the underlying assumption of using the force on a fixed cylinder instead of the true floating cylinder may not always be conservative. As an example of the approximation involved, Fig. 5 also shows the mean drift force on the OC3-Hywind platform; in this case the approximation is in fact conservative.

Using Equation (19), the integral in Equation (16) can be evaluated:

$$I = C^2 \int_{\omega_1}^{\omega_2} D^2(\omega) \mathrm{d}\omega \tag{21}$$

This integral must be evaluated in two parts, corresponding to the two asymptotes of Equation (20); depending on the relative values of the cylinder radius and the wave spectrum mean period, one or both parts are needed. The results are:

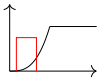

$$I = I_{L2} - I_{L1} = 1.70\, H_s^4 \omega_m^{11} (a/g)^6 \tag{22a}$$

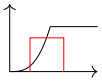

$$I = (I_{LX} - I_{L1}) + (I_{H2} - I_{HX}) = 1.40 \times 10^{-3}\, H_s^4 \left[\omega_m^{-1} - 0.412\, \omega_m^{-2} (a/g)^{-1/2} - 3.15 \times 10^{-8}\, \omega_m^{-13} (a/g)^6\right] \tag{22b}$$

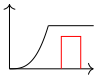

$$I = I_{H2} - I_{H1} = 1.18 \times 10^{-3}\, H_s^4 \omega_m^{-1} \tag{22c}$$

where I_{L1} is the value of the integral evaluated at ω_1 when this lies within the lower asymptote, I_{H1} is the corresponding value when ω_1 lies within the upper asymptote, I_{HX} is the value for the upper asymptote at ω_X, and so on.

Substituting Equations (14)–(22) into Equation (13) results in an expression for the slow drift standard deviation:

$$\sigma_x = \left(g\sqrt{\frac{2}{\pi}}\right) \zeta^{-1/2}\ \omega_n^{-3/2}\ d^{-1}\ H_s^2\ F(a, \omega_m) \tag{23}$$

where $F(a, \omega_m) = I^{1/2} a^{-1} H_s^{-2}$, and I is given in Equation (22). Equation (23) represents the main result of this paper: it predicts how the order of magnitude of the slow drift motion varies with both the structural and mooring properties (damping factor ζ, natural frequency in surge ω_n, platform size a and draft d), and the wave environment (significant wave height H_s and mean wave period ω_m).

The dependence on the platform radius a and mean wave period ω_m is relatively complex, described by the function $F(a,\omega_m)$, while the dependence on the other parameters is straightforward. Table 3 lists the results in the limits of very small and very large diameters when only one of the asymptotes of Equation (20) applies. The scaling at intermediate diameters can of course be determined from Equations (22) and (23) but takes a more complicated form.

The force function I and response function F are both plotted in the top row of Fig. 6. Overall, the slow drift force I increases with the cylinder diameter. The force is reduced for very low-frequency waves, because then the platform is small compared to the wavelength. Looking at the response function F in the top right of Fig. 6, different types of behaviour are seen at low and high frequencies. At low frequencies, the response increases with the size of the platform in the same way as the force. At high frequencies, the inertia of the platform becomes more important and the large inertia of large platforms causes the response to reduce as the size of the platform increases.

Typical mean wave frequencies in the North Sea might be roughly 0.5–0.8 rad s^{-1}, while in extreme conditions they may be 0.3–0.4 rad s^{-1} [2]. At the lower frequencies, the slow drift motion is predicted to decrease with diameter at all scales, supporting the original suggestion that smaller floating structures will experience smaller slow drift motions. At the higher frequencies, the picture is more complicated but at the scale of typical floating wind turbines, the same conclusion seems to hold.

According to Equation (23), the draft of the platform also has a significant effect. This seems relevant to the original example of the OC3-Hywind platform, which is a spar buoy with a very deep draft of 120 m. In the approximate result, the dependence on draft is purely through its effect on the platform inertia. In reality the mean drift force is also affected by draft, but this is not seen in the approximate results because the mean drift force is approximated by the mean drift force on a bottom-piercing fixed cylinder. The difference will be negligible for short waves (high ω_m) but for long waves (low ω_m) the force may be overestimated since part of the wave can pass below the platform.

3.2. Validity of approximations

In deriving the approximate result of Equation (23), eight main assumptions have been made:

1. *Only cylindrical platforms are considered.* Although this is a limitation, many platforms are indeed cylindrical.
2. *Only surge motion is allowed.* For floating offshore systems it is usual for the peak mooring line forces to be dominated by the second order motions in surge, sway and yaw. The present analysis is concerned predominantly with the surge motion of a floating turbine, and it address the question of whether second order slow drift motion is significant for this type of system.

Table 3
Scaling of slow drift response σ_x with various parameters in the limits of small and large diameter platforms.

Parameter	Small diameter Low frequency	Large diameter High frequency
Platform radius	a^2	a^{-1}
Mean wave frequency	$\omega_m^{11/2}$	$\omega_m^{-1/2}$
Damping factor	$\zeta^{-1/2}$	
Natural frequency	$\omega_n^{-3/2}$	
Significant wave height	H_s^2	
Platform draft	d^{-1}	

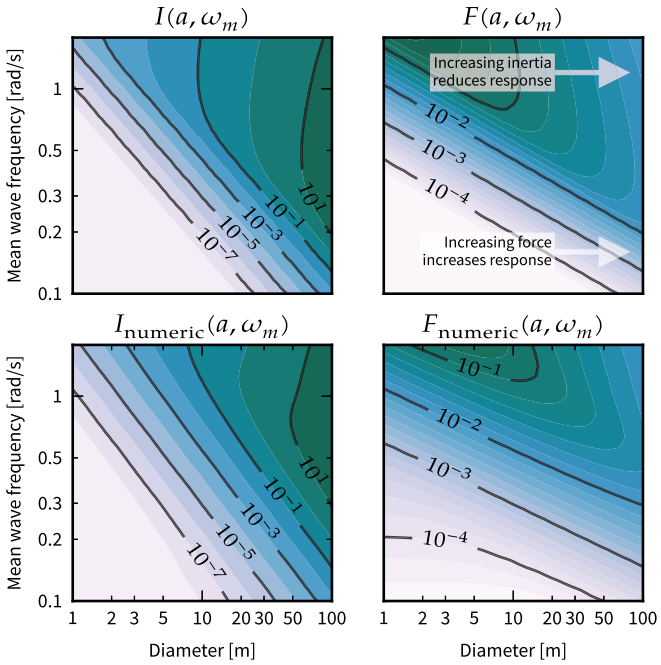

Fig. 6. Left: slow drift force integral *I*. Right: slow drift response function *F*. Top row: analytical results with rectangular spectrum approximation and mean drift force asymptotes. Bottom row: numerical results with ISSC spectrum and mean drift force on fixed cylinder. All scales are logarithmic.

Other components of the turbine motion, for example pitch, will affect other aspects of the system performance and design, although this is beyond the main scope of the present work. Low frequency second order motions in degrees of freedom other than surge, were these of interest, could be readily be investigated by using the present methodology.

3. *Natural frequency and damping are assumed constant for any size of platform.* This is reasonable in that natural frequencies are usually chosen to be far away from the main wave-frequency forcing, which is independent of platform size.
4. *The natural frequency is assumed to be small and damping is assumed to be light*, where 'small' implies that $\boldsymbol{S}_{FF}^{(2)}(\omega_n) \approx \boldsymbol{S}_{FF}^{(2)}(0)$.
5. *The mean surge force on the floating platform is approximated by the mean surge force on a fixed bottom-piercing cylinder of the same diameter.* The impact of this and the previous assumption will be illustrated for one particular case in the next section.
6. *The mean surge force on the fixed cylinder is approximated by its two asymptotes.* …
7. *The wave spectrum is approximated by the rectangular spectrum.* These two can easily be assessed by numerically calculating the integral *I* using the original ISSC wave spectrum and the fixed cylinder mean drift force, rather than using the rectangular approximation and the mean drift force asymptotes of Fig. 5. The results of the latter are shown in the top part of Fig. 6 and were described above; the results of the former are shown in the bottom part of Fig. 6. Compared to the numerical solution, the approximations over-predict the response for moderate diameters and wave frequencies. Fig. 7 shows this more clearly. Since the approximate results are conservative by a factor of 3 or less, the use of the results to estimate the scaling of the slow drift motion is justified.
8. *Added mass is neglected.* Inertial forces are small at the low frequencies of interest here; in any case, neglecting the added mass is a conservative assumption.

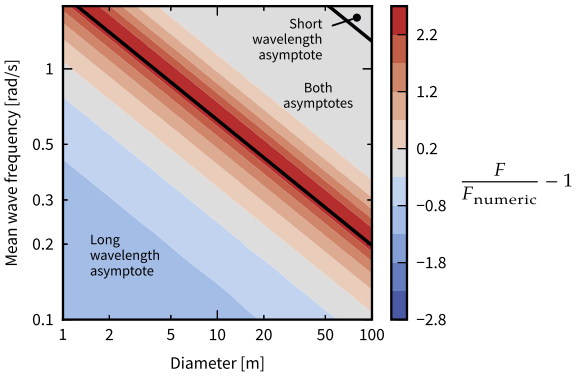

Fig. 7. Error due to rectangular spectrum and mean drift force asymptotes. The regions where the long- and short-wavelength asymptotes apply are also shown.

3.3. Numerical results for slow drift motion

Of the assumptions above, the impact of numbers 3 and 4 can be illustrated by calculating the full transfer function and second-order force spectrum for a particular case where data is available, the OC3-Hywind platform used previously. This platform is a spar buoy and has a diameter of 6.5 m at the waterline, tapering to 9.4 m diameter 12 m below the surface. This causes the actual mass of the platform to be roughly twice the value calculated by Equation (14), and this has been corrected for in the results which follow by modifying the estimated platform mass of Equation (14) to reflect the actual shape of the platform.

The slow drift motion standard deviation is found from Equations (4) and (5), as described in Section 2. To be consistent with the approximate results, only the surge degree of freedom is included.

The upper part of Fig. 8 compares the approximate slow drift standard deviation with the full numerical calculation, for the ISSC spectrum (Equation (17)). The difference between the results labelled 'analytical' and 'numerical' is the same as that discussed above and shown in Fig. 6: the rectangular approximation of the spectrum and the asymptotic mean drift force. The difference between the 'numerical' and 'full' curves is due mainly to the fact that the cylinder is not rigidly attached to the sea bed, and also the tapered shape. In this case, the 'numerical' results overestimate the slow drift motion by up to a factor of 10, and at worst the 'analytical' results overestimate the motion by an additional factor of 4. Note that the approximate results agree better than this within the range of typical wave frequencies (shaded). In particular, the motion predicted by all results is small in the storm wave range.

The lower part of Fig. 8 shows the approximate predictions for the three platform geometries listed in Table 4. The UMaine TLP has been included as it is the other platform studied by Roald et al. [8]. The Sevan FPSO [21] is included as an example of a much larger offshore floating structure. These results illustrate again the prediction of the approximate result that the slow drift motion of the larger structure is indeed larger than the smaller wind turbine platforms.

4. Conclusions

In this paper a frequency-domain model of a flexible floating wind turbine structure with first- and second-order hydrodynamic loading has been developed. Although previous work on frequency-domain modelling of floating wind turbines has neglected the structural dynamics of the turbine structure, this need not be the case.

A simplified analysis of the scaling of the second-order response

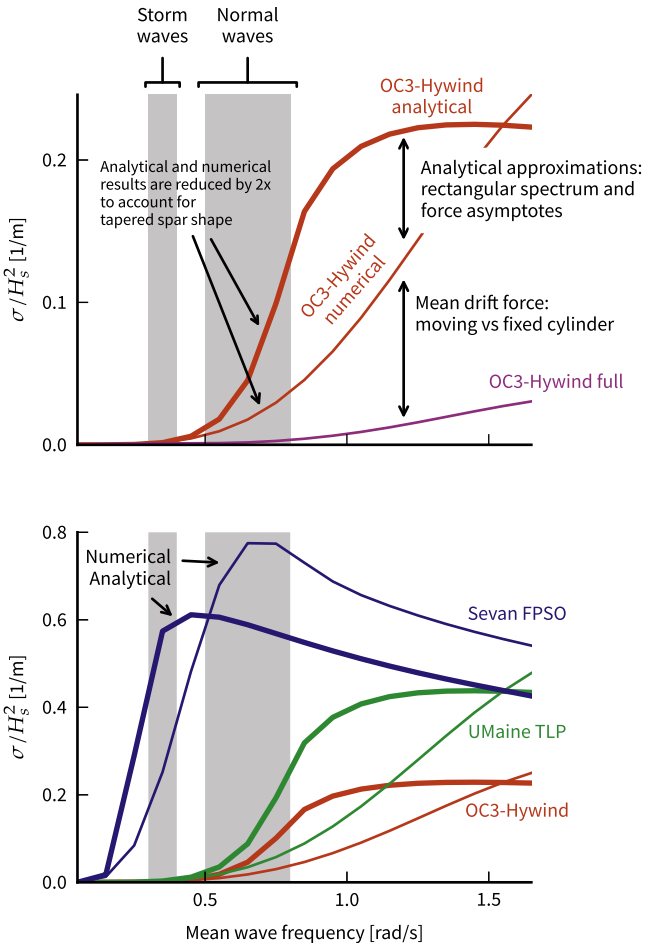

Fig. 8. Above: comparison of analytical and numerical results for the simple cylinder with actual numerical results for the OC3-Hywind platform. Below: analytical and numerical results for the three platform geometries listed in Table 4. The shaded bands show typical wave frequencies under storm and normal conditions [2].

Table 4
Example platform geometries. Damping for UMaine TLP and Sevan FPSO are assumed values.

Platform	Radius [m]	Draft [m]	ω_n [rad/s]	ζ
OC3-Hywind [5]	3.25	120.0	0.05	6%
UMaine TLP [20]	3.25	24.0	0.16	5%
Sevan FPSO [21]	30.00	17.0	0.053	5%

with the size of the platform was developed. Although the response depends on several parameters, within the main region of interest the second-order response is predicted to decrease with platform diameter. Since floating wind turbine platforms are generally smaller than other offshore floating structures, their second-order response may indeed be relatively small. This has implications for modelling, since if the second-order response is small, simplified and more efficient approaches are possible. The implications are also practical, since slow drift can be an important feature for the design of the floating platform.

Several assumptions and approximations were made in order to derive a closed-form result. Limited data is available to verify the error introduced by these approximations; in the one available case, the approximate result is conservative by, at worst, a factor of 40. More data is needed to determine to what extent the simplified analysis represents actual floating wind turbine platforms. It may also be possible to relax some of the assumptions to give better estimates of the slow drift response.

Acknowledgements

This work was funded by an EPSRC doctoral training award (ref. 1089390) and supported by GL Garrad Hassan.

References

[1] R. Lupton, Frequency-domain Modelling of Floating Wind Turbines, 2014. Ph.D. thesis.
[2] O.M. Faltinsen, Sea Loads on Ships and Offshore Structures, Cambridge University Press, 1993.
[3] N. Barltrop, Floating Structures: a Guide for Design and Analysis, The Centre for Marine and Petroleum Technology, 1998.
[4] J. Lucas, Upwind Project: Comparison of First and Second Hydrodynamic-results for Floating Offshore Wind Structures, Tech. Rep., Garrad Hassan, 2011.
[5] J. Jonkman, Definition of the Floating System for Phase IV of OC3, Tech. Rep. NREL/TP-500–47535, National Renewable Energy Laboratory, Golden, USA, 2010.
[6] Wamit Inc, WAMIT User Manual, Version 6.4, 2002. Tech. rep.
[7] A. J. Goupee, B. J. Koo, R. W. Kimball, K. F. Lambrakos, H. J. Dagher, Experimental comparison of three floating wind turbine concepts J. Offshore Mech. Arct. Eng. 136 (2) 020906–020906. http://dx.doi.org/10.1115/1.4025804.
[8] L. Roald, J. Jonkman, A.N. Robertson, N. Chokani, The effect of second-order hydrodynamics on floating offshore wind turbines, in: Energy Procedia, vol. 00, Elsevier, Trondheim, 2013.
[9] J. Jonkman, M.L.J. Buhl, FAST Users' Guide, Tech. rep., NREL, 2005.
[10] T. Duarte, A.J.N.A. Sarmento, J. Jonkman, Effects of second-order hydrodynamic forces on floating offshore wind turbines, in: AIAA SciTech, no. April, National Harbour, Maryland, 2014.
[11] I. Bayati, J. Jonkman, A.N. Robertson, A. Platt, The effects of second-order hydrodynamics on a semisubmersible floating offshore wind turbine, J. Phys. Conf. Ser. 524 (2014) 012094, http://dx.doi.org/10.1088/1742-6596/524/1/012094.
[12] Y.K. Lin, Probabilistic Theory of Structural Dynamics, 1976.
[13] K. Worden, G. Tomlinson, Nonlinearity in Structural Dynamics, Taylor & Francis, 2000.
[14] R.S. Langley, Second order frequency domain analysis of moored vessels, Appl. Ocean Res. 9 (1) (1987) 7–18.
[15] J. Pinkster, Low Frequency Second Order Wave Exciting Forces on Floating Structures, Tech. rep., Netherlands Ship Model Basin, Wageningen, The Netherlands, 1980.
[16] J.A.P. Aranha, A.C. Fernades, On the second-order slow drift force spectrum, Appl. Ocean Res. 17 (1995) 311–313.
[17] S.K. Chakrabarti, Handbook of Offshore Engineering, Elsevier, 2005.
[18] K.R. Drake, An analytical approximation for the horizontal drift force acting on a deep draught spar in regular waves, Ocean. Eng. 38 (5–6) (2011) 810–814, http://dx.doi.org/10.1016/j.oceaneng.2011.02.003.
[19] R. Eatock Taylor, C.S. Hu, F.G. Nielsen, Mean drift forces on a slowly advancing vertical cylinder in long waves, Appl. Ocean Res. 12 (3) (1990) 141–152.
[20] A.N. Robertson, J. Jonkman, Loads analysis of several offshore floating wind turbine concepts, in: Proceedings of the 21st International Offshore and Polar Engineering Conference, Maui, Hawaii, 2011, pp. 443–450.
[21] Y. Zhang, Response Statistics of a Floating Vessel in Spreading Seas, Ph.D. thesis, University of Cambridge, 2010.